# Reduction of microkinetic reaction models for reactor optimization exemplified for hydrogen production from methane

Florian Karst [a], Matteo Maestri [b], Hannsjörg Freund [c], Kai Sundmacher [a,d,∗]

[a] Max Planck Institute for Dynamics of Complex Technical Systems, Sandtorstr. 1, 39106 Magdeburg, Germany
[b] Laboratory of Catalysis and Catalytic Processes, Dipartimento di Energia, Politecnico di Milano, Piazza Leonardo da Vinci 32, 20133 Milano, Italy
[c] Institute of Chemical Reaction Engineering, Friedrich-Alexander-University Erlangen-Nuremberg, Egerlandstr. 3, 91058 Erlangen, Germany
[d] Institute for Process Engineering, Otto von Guericke University, Universitätsplatz 2, 39106 Magdeburg, Germany

## HIGHLIGHTS

- We present a new reduction technique for complex chemical reaction networks.
- This easy-to-use method is universal and ensures conservation of mass.
- We exemplify the reduction technique for a C1 microkinetic reaction network.
- The significantly reduced reaction network shows still an excellent agreement.

## ARTICLE INFO

## ABSTRACT

Sustainable and efficient processes require optimal design and operating conditions. The determination of optimal process routes, however, is a challenging task. Either the models and underlying chemical reaction rate equations are not able to describe the process in a wide ranges of reaction conditions and thus limit the optimization space, or the models are too complex and numerically challenging to be used in dynamic optimization. To address this problem, in this contribution, a reduction technique for chemical reaction networks is proposed. It focuses on the sensitivity of the reaction kinetic model with respect to the removal of selected reaction steps and evaluates their significance for the prediction of the overall system behavior. The method is demonstrated for a $C_1$ microkinetic model describing methane conversion to syngas on $Rh/Al_2O_3$ as catalyst. The original and the reduced microkinetic model show excellent qualitative and quantitative agreement. Subsequently, the reduced kinetic model is used for the optimization of a methane reformer to produce a hydrogen rich gas mixture as feed for polymer electrolyte membrane (PEM) fuel cell applications.
© 2015 The Authors. Published by Elsevier B.V. This is an open access article under the CC BY license (http://creativecommons.org/licenses/by/4.0/).

## 1. Introduction

As economical and ecological aspects play a significant role in the design of chemical production processes, model-based optimization is crucial for the rational derivation of the best process route and optimal equipment for efficient and sustainable production [1,2].

Reliable process optimization requires quantitative and sufficiently accurate information about the underlying physical and chemical phenomena. With increasing computational power, new theoretical approaches and advanced numerical algorithms, it is now possible to use microkinetic multi-step descriptions of chemical reactions, based on first principles, for reaction engineering purposes. Today, such microkinetic models for reaction systems with small molecules, e.g. ammonia [3] and nitrogen oxides [4–6] have been derived. Recently, the interest in $C_1$ chemistry, especially methane conversion into syngas components, has grown considerably. Microkinetic models for methane catalytic partial oxidation [7], reforming [8–11], oxidative coupling [12], and $CO/H_2$ oxidation [13] are available, but also models that are able to deal with multiple chemical regimes for methane conversion at the same time [14–17].

But the high complexity of detailed microkinetic reaction models turned out to be a challenging feature, especially for model-based reactor optimization. The microkinetic rate

∗ Corresponding author at: Max Planck Institute for Dynamics of Complex Technical Systems, Sandtorstr. 1, 39106 Magdeburg, Germany.
E-mail addresses: karst@mpi-magdeburg.mpg.de (F. Karst), matteo.maestri@polimi.it (M. Maestri), hannsjoerg.freund@crt.cbi.uni-erlangen.de (H. Freund), sundmacher@mpi-magdeburg.mpg.de (K. Sundmacher).

**Notation**

*Latin*

| Symbol | Description (unit) |
|---|---|
| $A$ | pre-exponential factor (– or 1/s) |
| $a$ | specific surface area $\left(\frac{1}{m}\right)$ |
| $c_i$ | concentration of component $i$ $\left(\frac{mol}{m^3}\right)$ |
| $\hat{c}_i = \frac{c_i}{c_{t,0}^g}$ | dimensionless concentration of component $i$ (–) |
| $D_i$ | diffusion coefficient of component $i$ $\left(\frac{m^2}{s}\right)$ |
| $E_A$ | activation energy $\left(\frac{J}{mol}\right)$ |
| $\hat{j}_i = \frac{j_i}{c_{t,0}^g k_m^{ref}}$ | dimensionless external molar dosing flux (–) |
| $k$ | reaction rate constant (reaction specific) |
| $k_m$ | mass transfer coefficient $\left(\frac{m}{s}\right)$ |
| $\hat{k}_m = \frac{k_m}{k_m^{ref}}$ | dimensionless mass coefficient (–) |
| $M_i$ | molar mass $\left(\frac{kg}{mol}\right)$ |
| $N$ | number of …(–) |
| $n$ | molar mass flux $\left(\frac{mol}{s}\right)$ |
| $\hat{n} = \frac{n}{c_{t,0}^g k_m^{ref}}$ | dimensionless molar mass transfer flux (–) |
| $n_{Sc}$ | exponent of Schmidt-number in Sherwood-correlation $(Sh = K_{Sh} Re^{n_{Re}} Sc^{n_{Sc}})$ (–) |
| $p$ | total pressure (Pa) |
| $R$ | universal gas constant $\left(\frac{J}{molK}\right)$ |
| $r_j$ | rate of reaction $j$ $\left(\frac{mol}{m^2 s}\right)$ |
| $T$ | temperature (K) |
| $t$ | time (s) |
| $x_i$ | molar fraction of component $i$ (–) |

*Greek*

| | |
|---|---|
| $\Gamma_{Rh}$ | active site density $\left(\frac{mol}{m^2}\right)$ |
| $\epsilon$ | error (–) |
| $\epsilon$ | void fraction (–) |
| $\Theta$ | surface coverage (–) |
| $v_{i,j}$ | stoichiometric coefficient of component $i$ in reaction $j$ (–) |
| $\sigma_i$ | chemical production rate of component $i$ $\left(\frac{kg}{m^2 s}\right)$ |
| $\tau = a^{gc} k_m^{ref} t$ | dimensionless time (–) |

*Superscripts*

| | |
|---|---|
| $c$ | catalyst |
| $g$ | gas phase |
| $gc$ | gas/catalyst interface |
| $k$ | index number |
| $ref$ | reference |

*Subscripts*

| | |
|---|---|
| 0 | initial state at $t = 0$ |
| *Com* | components |
| *final* | final state |
| $i$ | component index |
| $j$ | reaction index |
| *Re* | reactions |
| $t$ | total |

expressions are strongly nonlinear functions of temperature, gas phase concentrations and catalyst surface coverages and interdependent. Furthermore, the reaction rates often cover many orders of magnitude, which results in bad model scaling and ill-posed numerical problems. For this reason, comparative simulation studies [18–22], but only few rigorous optimizations are found in literature to improve the design of catalysts, reactors and processes. E.g., for the ammonia synthesis Jacobsen et al. [23] derived an optimal catalyst on the atomistic scale based on volcano curves computed from first principles.

The objective of the present work is to combine microkinetic models and rigorous reactor optimization. To overcome the before mentioned numerical issues, a new reduction technique for microkinetic reaction network models based on network-wide analysis of errors in the predicted reaction rates is proposed. Previous reduction techniques for chemical reaction networks are based on progressive species reduction with reparametrization [24], element flux analysis [25], integer linear programming [26], principle component analysis [27] and reaction route graphs [28–30].

Progressive species reduction with parametrization of the reaction rates uses a global error function to gradually reduce the number of species in the reaction model with element flux analysis. Afterward the model parameters are re-estimated within their uncertainty region using a genetic algorithm. Although this procedure opens a very elegant path for reparametrization of the reaction model, genetic algorithms need be used with great caution, as the results may strongly depend on the configuration of the genetic algorithm. This further increases computation and implementation complexity significantly. Element flux analysis considers the fluxes of one element, e.g. carbon, from one molecule to another and judges the significance of a reaction by comparing the magnitude of the element fluxes between different reactions. The larger the element flux, the more significant the reaction will be. However, this method requires the considered element to be present in every reaction. If this is not the case, this reaction cannot

be compared with the others properly. This limits the method to reaction systems that share a common element.

Reaction and species elimination with integer linear programming (ILP) is an automated, optimization-based reduction method. Besides integer formulation that is in general hard to handle, this method requires additional solvers and optimization routines. Furthermore, the mass balance of the reduced system is not ensured.

From a systems engineering point of view, the reaction route graphs are very fascinating. The authors [28–30] established an analogy between reaction networks and electrical circuits. By considering reactions as chemical resistors, this information can be used to identify major barriers within the reaction network. In analogy to electrical engineering, they are able to use this information to derive a chemical reaction that behaves as an equivalent resistance. For small systems, the authors were even able to determine analytical solutions. Unfortunately, this method is difficult to use for complex chemical reaction networks, as the determination of the reaction route graphs is very difficult.

All these previous approaches are not fully suitable for use in rigorous dynamic optimization, where universal and computationally cheap methods are desirable. To avoid reparametrization issues and complex numerical methods, we here aim for an easy-to-use reduction approach based on sensitivity analysis that does not require special network properties or problem statements.

The present work is structured as follows. First, a methodology for preprocessing and reduction of a given microkinetic model is derived, demonstrated and discussed in detail. For these purposes, the microkinetic model proposed by Maestri et al. [14], which describes the conversion of methane to syngas components on Rh/Al$_2$O$_3$ as catalyst, is used as example of industrial relevance. In the second step, a validation of the reduced kinetic model is carried out. Finally, the reduced kinetic model is utilized for rigorous reactor optimization. For this purpose, we apply the Elementary Process Functions (EPF) methodology proposed by our group [1,2].

## 2. Kinetic modeling for reactor optimization

### 2.1. Selection of kinetic model

In heterogeneous catalysis, one has to differentiate between macro and microkinetics. Microkinetic models describe reaction kinetics at the catalyst, without any interference from internal or external transport phenomena, while macrokinetic models represent a combination of heat and/or mass transport and chemical reaction. In rigorous process optimization over wide operating conditions, microkinetic models are preferable, because the reaction kinetic parameters are not masked by transport effects and therefore valid within a broad range of reaction conditions.

Within microkinetic models, elementary and lumped rate expressions have to be differentiated. Elementary microkinetic models aim to represent all mechanistic reaction steps and thus take intermediates of the surface chemistry into account. Lumped models (e.g. Langmuir–Hinshelwood or Eley–Rideal) on the other hand involve simplifications (e.g. quasi-stationarity, rate determining step (RDS), and most abundant surface intermediate (MASI)). For this reason, elementary step models offer a more fundamental understanding of the molecular processes taking place on the catalyst surface. However, even for simple reaction systems with small molecules and few species, elementary microkinetic reaction models often result in large-scale networks, due to the large number of species considered and multiple reaction pathways. Microkinetic networks often suffer from bad scaling behavior, because under certain reaction conditions parts of the network are almost or completely inactive. Moreover, compared to lumped kinetics, a much higher number of kinetic parameters has to be identified. But, elementary microkinetic models allow for an accurate description of the chemical system over large ranges of concentration, pressure and temperature, since no rate determining step is assumed [31]. This is an essential property for the optimization of chemical reactors, as it is in general not known a priori in which range of operating conditions the optimal process performance can be achieved. On the other hand, large scale, strongly nonlinear, and badly scaled kinetic models can cause problems when it comes to optimization.

Therefore, a compromise between elementary microkinetics and lumped models, while still of much higher level of detail and complexity than traditional kinetic approaches such as, e.g.,

Eley–Rideal or Langmuir–Hinshelwood is needed for rigorous reactor optimization. Thus, the key element is the reduction of microkinetic models to obtain more compact kinetic models that are still valid over a large range of reaction conditions. For this purpose, we identify a subset of the full microkinetic reaction network which contains the most significant elementary steps.

### 2.2. Reduction approach

The general steady state mass balance on the catalyst surface at a given gas phase concentration $c_i^g$ can be formulated as follows:

$$0 = \mathbf{N}\mathbf{r}(\mathbf{c^g}, T, \mathbf{\Theta}) \quad \text{with } \mathbf{N} = [v_{i,j}], \ \mathbf{r} = (r_j), \ \mathbf{c^g} = (c_i^g), \ \mathbf{\Theta} = (\Theta_i)$$

(1)

where $v_{i,j}$ is the coefficient of species $i$ in reaction $j$, and $r_j$ the rate of reaction $j$. All reactions are considered reversible, characterized by a forward $r_{j,f}$ and backward reaction $r_{j,b}$.

$$r_j = r_{j,f} - r_{j,b}$$

(2)

The here proposed model reduction technique is based on the recalculation of the flux distribution in the network, when a reaction $(k)$ is removed from the network. The remaining reaction rates $\left(r_j^k\right)$ must ensure that the component mass balances are fulfilled, Eq. (1). As a consequence, the individual reaction rates change from $(r_j)$ to $\left(r_j^k\right)$ due to a different flux distribution inside the network to compensate for the 'removed' reaction. The kinetic parameters of the original model are reused. These mass balances in terms of the reduced network sound as follows:

$$0 = \mathbf{N^k}\mathbf{r^k}(\mathbf{c^g}, T, \mathbf{\Theta^k})$$

(3)

where the superscript $k$ denotes the removed reaction $k$.

Now, we calculate the error $\epsilon^k$ between the original and the reduced model as a sum of all deviations in the reaction rates.

$$\epsilon^k = \frac{\sum_{j=1}^{N_{Re}} \left(r_j - r_j^k\right)^2}{s^k}$$

(4)

To make the errors $\epsilon^k$ comparable for different reaction conditions (e.g. temperature), all values are scaled by the variance $s^k$ of the recalculated rates $r_j^k$.
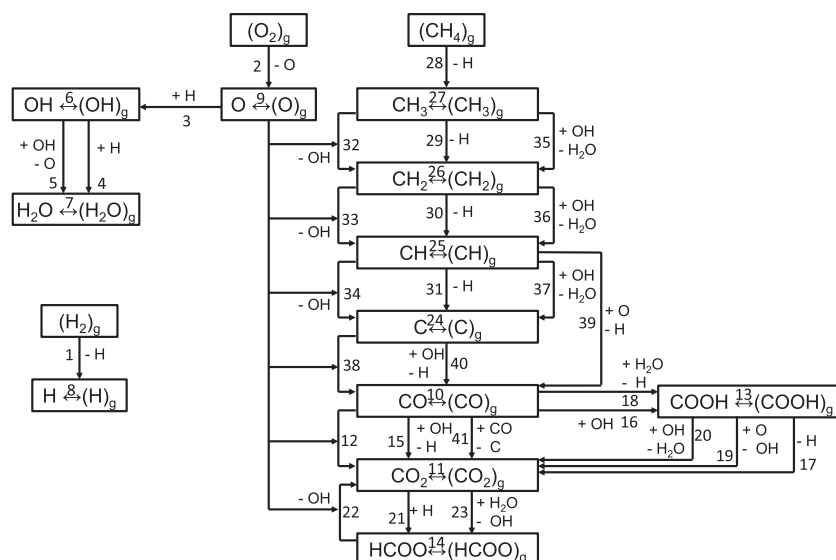


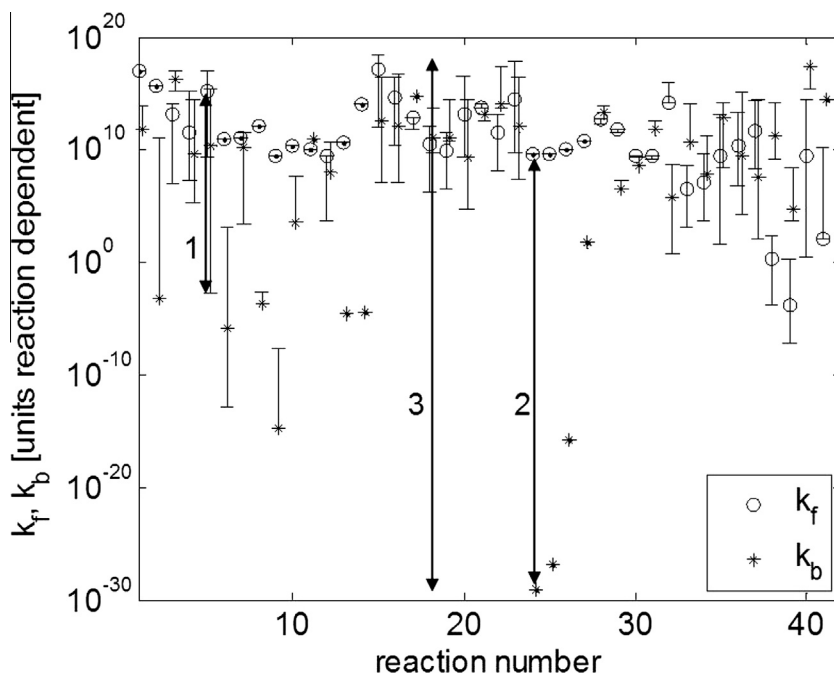**Fig. 1.** Scheme of the original microkinetic reaction network for $C_1$ chemistry [14].

**Fig. 2.** Parameter ranges at different surface coverages/compositions for the reaction rate constants at 800 K. ○ and ★ represent the parameters for an uncovered surface. (1) 16 orders of magnitude coverage dependence; (2) 38 orders of magnitude for forward/backward reaction; (3) 45 orders of magnitude covered overall.

$$s^k = \frac{\sum_{j=1}^{N_{Re}} \left( r_j^k - \bar{r}^k \right)^2}{N_{Re} - 1} \qquad (5)$$

The average reaction rate $\bar{r}^k$ is calculated from the following equation.

$$\bar{r}^k = \frac{\sum_{j=1}^{N_{Re}} r_j^k}{N_{Re}} \qquad (6)$$

If the cancellation of reaction $k$ yields a large error $\epsilon^k$, this reaction was important for the network, because it can only be compensated by a large change in the flux distribution inside the network. Therefore, this reaction is considered to be significant and thus cannot be removed from the network. Consequently, only reactions that yield small deviations from the flux distribution of the original model are removable. These reactions need to fulfill the following condition

$$\epsilon^k \leqslant \epsilon^{max} \qquad (7)$$

where $\epsilon^{max}$ is the maximum error bound. This is a user-defined threshold to steer the degree of reduction. If a large error $\epsilon^{max}$ is allowed, this will yield a strongly reduced and quickly computable, but less accurate kinetic model.

The model reduction method sketched above has several features. First, it is neither dependent on the original network structure nor on any particular formulation of the reaction rates and thus is applicable to any microkinetic model. Second, it focuses directly on the actual fluxes in the network, rather than the concentrations or other measures and fulfills the mass balances by calculating the resulting flux redistribution in the network. Third, only one parameter ($\epsilon^{max}$) is needed to be specified, which makes the concept user friendly and quite easy to use.

The intrinsic nature of this method is to identify non-significant edges of the network graph at given reaction conditions to obtain a reduced model at a defined error. If several reaction conditions (e.g. pressures, temperatures, and chemical regimes) shall be taken into consideration, the reduction approach must be applied for all those conditions individually. As the balance equations have to be
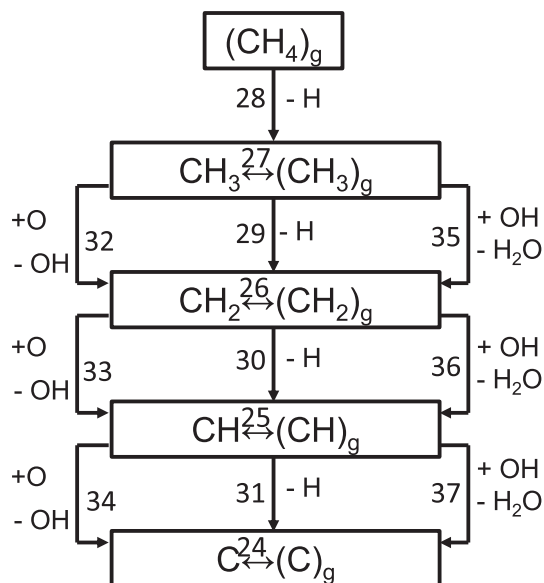


**Fig. 3.** Considered sub-network for the dehydrogenation of methane.

satisfied for every calculation, the determination of the errors can be computationally demanding for systems with a very high number of reactions. Of course, one can use advanced methods for the optimal design of experiments in order to determine a minimum set of in-silico experiments to reduce this computational effort.

Usually, the computationally most demanding part in the reduction framework is to solve the mass balance (Eq. (1)). As every reaction in the reaction network needs be perturbed, the mass balance must be solved ($N_{Re} + 1$) times. If all reaction rates (original and perturbed) from Eq. (1) are known, the reduction approach is executed by calculating the reaction rate errors (Eqs. (4)–(6)) and verifying the reaction significance with Eq. (7). These equations are easy to implement and computationally

**Table 1**
Reduction method exemplified for dehydrogenation of methane under catalytic partial oxidation reaction conditions at 800 K.

| $j$ | $r_j \left[\frac{mol}{m^2 s}\right]$ | $r_j^{24} \left[\frac{mol}{m^2 s}\right]$ | $r_j^{25} \left[\frac{mol}{m^2 s}\right]$ | $r_j^{26} \left[\frac{mol}{m^2 s}\right]$ | $r_j^{27} \left[\frac{mol}{m^2 s}\right]$ | $r_j^{28} \left[\frac{mol}{m^2 s}\right]$ | $r_j^{29} \left[\frac{mol}{m^2 s}\right]$ | $r_j^{30} \left[\frac{mol}{m^2 s}\right]$ | $r_j^{31} \left[\frac{mol}{m^2 s}\right]$ | $r_j^{32} \left[\frac{mol}{m^2 s}\right]$ | $r_j^{33} \left[\frac{mol}{m^2 s}\right]$ | $r_j^{34} \left[\frac{mol}{m^2 s}\right]$ | $r_j^{35} \left[\frac{mol}{m^2 s}\right]$ | $r_j^{36} \left[\frac{mol}{m^2 s}\right]$ | $r_j^{37} \left[\frac{mol}{m^2 s}\right]$ | $log_{10}(\epsilon^k)$ |
|---|---|---|---|---|---|---|---|---|---|---|---|---|---|---|---|---|
| 24 | -2.7e-25 | 0 | 5.3e-25 | -1e-25 | 3.5e-26 | -1.2e-42 | 4.4e-25 | 1.5e-24 | 4.7e-24 | 1.6e-25 | -1.4e-24 | -1e-24 | -2.6e-25 | -9e-25 | 4.3e-25 | -30 |
| 25 | -4e-24 | -2.6e-24 | 0 | -5.3e-24 | 2.9e-25 | 8.8e-51 | 8.3e-25 | 5e-25 | 2.5e-23 | -4e-24 | -2.3e-24 | 1.5e-24 | -6e-25 | -2.8e-24 | 3.8e-24 | -30 |
| 26 | -2.6e-24 | -1.4e-24 | -1.4e-24 | 0 | 4.6e-25 | -1e-55 | -1.3e-25 | -8.4e-25 | 2.7e-24 | -5.8e-25 | -1.1e-24 | -1.2e-24 | 1.4e-24 | -1.1e-23 | -4.4e-24 | -30 |
| 27 | -1.7e-12 | -1.7e-12 | -1.7e-12 | -1.7e-12 | 0 | -4.4e-49 | -1.7e-12 | -1.7e-12 | -1.7e-12 | -1.7e-12 | -1.7e-12 | -1.7e-12 | -4.5e-10 | -2.3e-12 | -1.7e-12 | -18 |
| 28 | 7.2e-04 | 7.2e-04 | 7.2e-04 | 7.2e-04 | 7.2e-04 | 0 | 7.2e-04 | 7.2e-04 | 7.3e-04 | 7.2e-04 | 7.2e-04 | 7.2e-04 | 1.5e-04 | 7.3e-04 | 7.3e-04 | -0.47 |
| 29 | 3.6e-07 | 3.6e-07 | 3.6e-07 | 3.6e-07 | 3.6e-07 | -2.1e-43 | 0 | 3.6e-07 | 3.5e-07 | 3.6e-07 | 3.6e-07 | 3.6e-07 | 9.5e-05 | 3.3e-07 | 3.5e-07 | -7.3 |
| 30 | 5.5e-06 | 5.5e-06 | 5.5e-06 | 5.5e-06 | 5.5e-06 | -4.6e-34 | 5.5e-06 | 0 | 4.7e-06 | 5.5e-06 | 5.5e-06 | 5.5e-06 | 1.2e-06 | 6.4e-04 | 4.5e-06 | -5 |
| 31 | 3.5e-04 | 3.5e-04 | 3.5e-04 | 3.5e-04 | 3.5e-04 | -6.2e-27 | 3.5e-04 | 3.5e-04 | 0 | 3.5e-04 | 3.5e-04 | 3.5e-04 | 7.4e-05 | 3.4e-04 | 7.3e-04 | -1.3 |
| 32 | 2.3e-07 | 2.3e-07 | 2.3e-07 | 2.3e-07 | 2.3e-07 | -5.3e-43 | 2.3e-07 | 2.3e-07 | 2.5e-07 | 0 | 2.3e-07 | 2.3e-07 | 5.9e-05 | 2.6e-07 | 2.6e-07 | -7.7 |
| 33 | -6.7e-07 | -6.7e-07 | -6.7e-07 | -6.7e-07 | -6.7e-07 | 5.4e-32 | -6.7e-07 | -6.7e-07 | -6.6e-07 | -6.7e-07 | 0 | -6.7e-07 | -1.4e-07 | -8.3e-05 | -6.6e-07 | -6.8 |
| 34 | -7.6e-08 | -7.6e-08 | -7.6e-08 | -7.6e-08 | -7.6e-08 | 2.9e-27 | -7.6e-08 | -7.6e-08 | -1.5e-07 | -7.6e-08 | -7.6e-08 | 0 | -1.6e-08 | -8.5e-08 | -1.8e-07 | -8.8 |
| 35 | -7.2e-04 | -7.2e-04 | -7.2e-04 | -7.2e-04 | -7.2e-04 | -7.4e-43 | -7.2e-04 | -7.2e-04 | -7.3e-04 | -7.2e-04 | -7.2e-04 | -7.2e-04 | 0 | -7.3e-04 | -7.3e-04 | -0.6 |
| 36 | -7.2e-04 | -7.2e-04 | -7.2e-04 | -7.2e-04 | -7.2e-04 | -5.4e-32 | -7.2e-04 | -7.2e-04 | -7.3e-04 | -7.2e-04 | -7.2e-04 | -7.2e-04 | -1.5e-04 | 0 | -7.2e-04 | -0.76 |
| 37 | -3.8e-04 | -3.8e-04 | -3.8e-04 | -3.8e-04 | -3.8e-04 | -9.7e-27 | -3.8e-04 | -3.8e-04 | -7.3e-04 | -3.8e-04 | -3.8e-04 | -3.8e-04 | -8e-05 | -3.9e-04 | 0 | -1.3 |
| $\bar{r}^k$ | | -5.3e-05 | -5.3e-05 | -5.3e-05 | -5.3e-05 | -9.4e-28 | -5.3e-05 | -5.4e-05 | -1.0e-04 | -5.3e-05 | -5.3e-05 | -5.3e-05 | 1.1e-05 | 3.7e-05 | 7.1e-07 | |
| $s^k$ | | 3.9e-07 | 3.9e-07 | 3.9e-07 | 3.9e-07 | 3.1e-07 | 3.9e-07 | 3.8e-07 | 3.5e-07 | 3.9e-07 | 3.9e-07 | 3.9e-07 | 3.2e-07 | 4.8e-07 | 4.7e-07 | |

inexpensive. Assuming that the major calculation time is consumed to solve the mass balance (Eq. (1)), the computational effort for the presented method scales linearly with the size of the reaction network. Therefore, the required computation time can be estimated to

$$t_{total} = DOF(N_{Re} + 1) * t_{calc} \qquad (8)$$

where $t_{total}$ is the overall computation time, $DOF$ the degrees of freedom, $N_{Re}$ the total number of reactions and $t_{calc}$ the typical time required to solve the mass balance (Eq. (1)). The degrees of freedom ($DOF$) are the number of all investigated reaction conditions. In case only one temperature, pressure and composition is considered, $DOF = 1$. If, however, three different temperatures, two pressures and five different compositions shall be examined, the degrees of freedom increase to $DOF = 3 * 2 * 5 = 30$. Using Eq. (8) one can already estimate the computational effort a priori and plan the number of investigated reaction conditions accordingly in order to find a reasonable compromise between computational effort and validity of the reduced network for different reaction conditions.

### 2.3. Demonstration example

To describe the mechanism of the conversion of methane to syngas, the $C_1$ microkinetic model from Maestri et al. [14] is used. This model is able to describe several chemical regimes, namely methane steam and dry reforming, catalytic partial oxidation, hydrogen and carbon monoxide combustion and water gas shift, on a $Al_2O_3$ supported rhodium catalyst. It was derived from first principles, combined with semi-empirical methods and experimental data. The model is thermodynamically consistent and applicable in a large range of temperatures (500–1150 K).

The full scale reaction network is shown in Fig. 1. It consists of 12 adsorbed species, free active surface sites (not shown in Fig. 1) gas phase species. Hydrogen, oxygen, and methane are assumed to adsorb dissociatively on the catalyst surface. The species are connected by 41 reversible reactions, including adsorption/desorption and surface reaction steps.

The microkinetic reaction rate of each elementary reaction step is formulated as a power law where the stoichiometric coefficients of the species participating in this step are used as reaction orders.

$$r_j = k_j c_{gasspecies}^{-\nu_{gasspecies,j}} \prod_{i=1}^{N_{COM}} \Theta_i^{-\nu_{i,j}} \quad \text{(chemisorption)} \qquad (9)$$

$$r_j = k_j \prod_{i=1}^{N_{COM}} \Theta_i^{-\nu_{i,j}} \quad \text{(surface reaction)} \qquad (10)$$

The rate constants $k_j$ are determined from the following equations:

$$k_j = s_j \sqrt{\frac{RT}{2\pi M}} \left(\frac{T}{T_0}\right)^{\beta_j} \exp\left(-\frac{E_{A,j}(\Theta, T)}{RT}\right) \quad \text{(chemisorption)} \qquad (11)$$

$$k_j = A_j \Gamma_{Rh} \left(\frac{T}{T_0}\right)^{\beta_j} \exp\left(-\frac{E_{A,j}(\Theta, T)}{RT}\right) \quad \text{(surface reaction)} \qquad (12)$$

One reason for the high accuracy of the here considered $C_1$ microkinetic model is the fact that the activation energies are not constant, but temperature and coverage dependent functions. For the detailed formulation of these functions the reader is referred to [14]. From the numerical point of view coverage-dependent activation energies are difficult, since they introduce additional nonlinear dependencies into the balance equations. To demonstrate this issue the rate constants were calculated at 800 K. In Fig. 2 the ranges of possible values for the forward and backward rate constant due to composition changes on the catalyst surface are depicted.

At low surface coverage (no influence of adsorbed species on activation energies) the rate constants in the network already vary over 45 orders of magnitude. While most rate constants feature values between $10^0 \, s^{-1}$ and $10^{17} \, s^{-1}$, some rate constants are very small, e.g. carbon desorption from the surface ($10^{-29} \, s^{-1}$; reaction 24). Also, the forward and backward rate constants can differ significantly, such that the related reactions are quasi-irreversible either in forward or backward direction. For carbon ad-/desorption the difference of the rate constants covers 38 orders
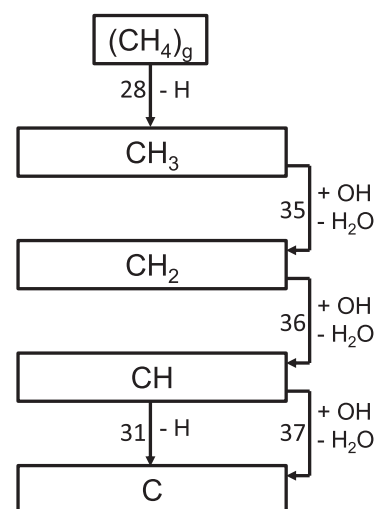


**Fig. 4.** Reduced reaction network for dehydrogenation of methane under catalytic partial oxidation conditions at 800 K.
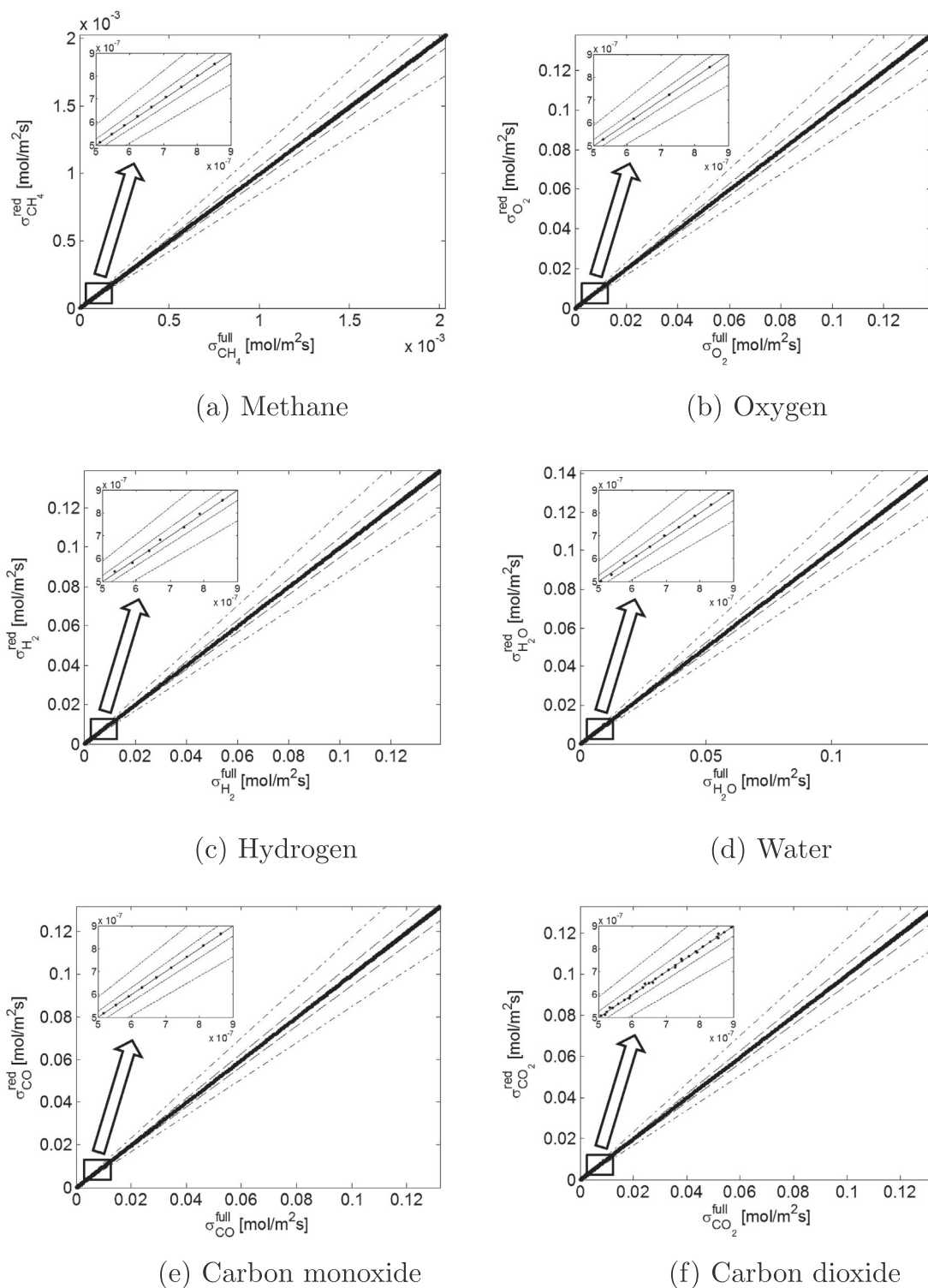
**Table 2**
Considered chemical regimes for the reduction of the microkinetic model and their assumed representative gas phase compositions.

| Regime | $x_{CH_4}$ | $x_{O_2}$ | $x_{H_2}$ | $x_{H_2O}$ | $x_{CO}$ | $x_{CO_2}$ |
|--------|------------|-----------|-----------|------------|----------|------------|
| CPO | 0.55 | 0.27 | 0.12 | 0.0 | 0.06 | 0.0 |
| SR | 0.41 | 0.0 | 0.14 | 0.41 | 0.05 | 0.0 |
| DR | 0.41 | 0.0 | 0.09 | 0.0 | 0.09 | 0.41 |
| WGS | 0.0 | 0.0 | 0.25 | 0.25 | 0.25 | 0.25 |
| HC | 0.0 | 0.31 | 0.62 | 0.07 | 0.0 | 0.0 |
| CC | 0.0 | 0.31 | 0.0 | 0.0 | 0.62 | 0.07 |
| ALL | 0.17 | 0.17 | 0.17 | 0.17 | 0.16 | 0.16 |

of magnitude. Furthermore, for a single reaction, the species adsorbed on the catalyst also have a significant influence on the rate constants. As shown in the Fig. 2, reaction 5 ($2OH_s \leftrightarrow H_2O_s + O_s$) depends strongly (16 orders of magnitude) on the amount of species adsorbed on the catalyst. Not shown here is the influence of the temperature, which further changes the values of the rate constants drastically within the range of temperature relevant in a technical process (500–1150 K).

Due to the large span of rate constants, it is very challenging to use this complex microkinetic model for rigorous reactor simulation and even more difficult for reactor optimization. Therefore, the significance-based method presented in Section 2.2 was applied in order to reduce the $C_1$ microkinetic network model to a smaller set of reaction steps.

For illustration, first the method is demonstrated for a sub-network, namely the dehydrogenation of methane to carbon on the rhodium surface. The relevant reactions 24–37 of the full network are shown in Fig. 3.

The gas phase composition ($x_{CH_4} = 0.55$; $x_{O_2} = 0.27$; $x_{H_2} = 0.12$; $x_{H_2O} = 0.0$; $x_{CO} = 0.06$; $x_{CO_2} = 0.0$) and the temperature (800 K) were fixed. Table 1 summarizes the obtained results. In the first row, the reaction numbers according to Fig. 3 are listed. The second row shows the reaction rates of the original network $r_j$. The subsequent rows contain the recalculated distribution of reaction rates $r_j^k$, where the $k$th reaction is set to zero. The last two lines comprise the mean reaction rate $\bar{r}^k$ and the variance $s^k$. Finally, the errors $\epsilon^k$ are calculated according to Eq. (4) and listed in the last row.

To reduce the system we allowed a maximum error of $\epsilon^{max} = 1 \cdot 10^{-3}$. All errors larger than $\epsilon^{max}$ are highlighted with a gray background color in Table 1. From these results, one can conclude that, for the considered reaction conditions (i.e., temperature and the gas phase composition), the dehydrogenation of methane mainly proceeds via a surface reaction with the hydroxide ion accompanied by the generation of water. This pathway is much faster than the oxidative dehydrogenation or the direct dehydrogenation via hydrogen elimination, except the direct dehydrogenation of CH (reaction 31). Furthermore, the reduction method does not only identify the most significant reactions, but it also reveals species that are not crucial for the accurate description of the important chemical events on the surface. Considering the ad- and desorption reactions 24–27 of the radical gas phase species $(C)_g$, $(CH)_g$, $(CH_2)_g$, and $(CH_3)_g$, according to our method, these steps are also not important, thus they do not occur in the gas phase at the here considered reaction conditions. Therefore, the reaction steps 24–27 and also the above mentioned gas phase species are not taken into consideration in the reduced microkinetic reaction network. However, all adsorbed species are still required. The reduced network is shown in Fig. 4. In this sub-network, the number of reactions was reduced from 14 to 5 and the number of species from 9 to 5.

### 2.4. Case study: reduction of $C_1$ microkinetic model and validation

In the next step the complete original reaction network was reduced, which was carried out in the same way as for the dehydrogenation of methane shown in Section 2.3. The reduced reaction network should be capable of representing different reaction regimes being embedded in the original network, namely methane catalytic partial oxidation (CPO), steam (SR) and dry reforming (DR), water gas shift (WGS), hydrogen (HC) and carbon monoxide combustion (CC), and a regime that includes all major gas phase components (ALL) based on specified extent of reaction. The desired validity range of the reduced kinetic model with respect to temperature is 400–1200 K. In order to get an adequate representation, differently reduced networks for different chemical regimes have to be determined. Appropriate gas phase compositions were chosen at which different chemical regimes are



**Fig. 5.** Reduced microkinetic model for $C_1$ chemistry. Regimes: catalytic partial oxidation, steam reforming, dry reforming, water gas shift reaction, hydrogen combustion and carbon monoxide combustion for temperatures between 400 K and 1200 K

(a) Methane

(b) Oxygen

(c) Hydrogen

(d) Water

(e) Carbon monoxide

(f) Carbon dioxide

**Fig. 6.** Chemical production rates $\sigma_i$ for the original and reduced reaction kinetic model at 800 K. ($- -\ \pm 5\%$ error; $- \cdot -\ \pm 15\%$ error).

dominant (as shown in Fig. 2). As evaluation temperatures 400, 600, 800, 1000, and 1200 K were used (see Table 2).

For all these reaction conditions, the reduction method was applied. The results are shown in Tables A1–A7 of the appendix. For clarity, only the errors (common logarithm) of the reactions $log_{10}(\epsilon^k)$ are listed. Here, the same threshold for the error $\epsilon^{max} = 1 \cdot 10^{-3}$ was used as for the example system. Reactions that cause an error greater than $log_{10}(\epsilon^{max}) = -3$ are highlighted with a gray cell background. The individual reactions that are required for

each chemical regime within the considered temperature range are also highlighted in the first row. The original reaction network was reduced from 41 to 21 reactions (see Fig. 5). Due to the change of the network structure, some components are not connected to the network anymore. These isolated species were also deleted from the reaction network. Thereby, the number of components was reduced from 28 to 18.

To check the qualitative and quantitative agreement between the original and the reduced network, a simulation was performed,
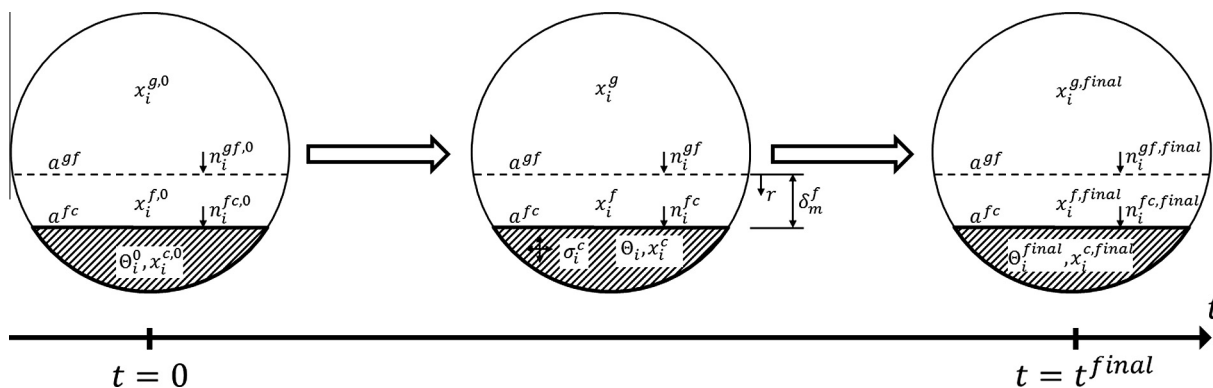
**Fig. 7.** Gas phase matter element moving through the process from time $t = 0$ up to the final residence time $t = t^{final}$. At each time step, the gas phase is in contact with the solid catalyst phase via a gas film.

where the kinetic behavior with identical conditions (inlet composition, temperature, pressure, ...) was compared. Here, we focus on the overall production rates for the dominant gas phase species ($CH_4$, $O_2$, $H_2$, $H_2O$, $CO$, $CO_2$). The simulation was carried out at 800 K for a chemical regime where all major gas phase components are present at equal molar amounts at the reactor inlet. The parity plots (Fig. 6) show excellent agreement between the original and the reduced model. All errors in the production rates of the species are below 5%. The maximum error is found at gas phase conditions with small hydrogen production rates (4.2% error) while the average error for hydrogen production was 0.07% and the overall average error was 0.05%. Also, for other chemical reaction regimes no larger error between the original and reduced microkinetic model was found.

### 2.5. Comparison with other reduction methods

Finally, we compare the here proposed 'reaction significance' based reduction method to alternative methods found in literature. In particular we consider Elementary Flux Analysis [25], Relative Production Rates and F-Test [32]. For all these methods, a reaction mechanism and a temperature have to be specified.

In Elementary Flux Analysis (EFA), the reactive fluxes (sources and sinks) for every atom (here: carbon, hydrogen, oxygen) are calculated and sorted in a descending order. Then, a user-defined cut-off is set (e.g. 1%) and all reactions below this cutoff are removed from the network.

The method of Relative Production Rates (RPR) is similar to Elementary Flux Analysis. However, here the focus is not on chemical elements, but on molecular species (e.g. methane, water, carbon dioxide). For every species, the total conversion rate (production and consumption) can be calculated. All reactions are considered to be important, whose magnitude relative to the total flux is larger than a user-defined threshold.

Using the F-Test, the significance of models and their parameters are judged. More detailed information is provided in [32].

Applying the before mentioned reduction techniques to the example system ($C_1$ microkinetic network) good agreement between the methods was achieved as shown in Table 3. Gray blocks represent the significant reactions for the different models, while non-significant reactions are white. The results of the here proposed method (reaction significance) are confirmed by at least two of the other reduction concepts, both for the significant and non-significant reactions. All other concepts show unique results (reaction that are significant or not), that differ in at least three reactions from our method and the others.

The concept of 'reaction significance' offers the advantage that it is a universal method and it is easy to implement. The interpretation of the results is straight forward. E.g., for EFA and RPR the case frequently occurs that a reaction is significant for a certain species but not for another and it remains unclear whether a reaction is really significant in this case. Furthermore, using the here proposed method, a reduction with respect to the number of reactions and components is achieved. For RPR this is not possible, because at least one reaction for the production of each species is kept. Using a user-defined threshold, there is only one degree of freedom to steer the degree of reduction, which directly indicates the obtained error in the overall flux distribution. In this regard, other methods focus on the magnitude of the individual reaction rates and their impact on the overall production rate for an element/component.

The F-test-significance is very low (here 20%) as no repetitive simulations with "experimental noise" are possible. Compared to optimal reduction concepts no MINLP optimization is required with all the additional difficulties that are introduced by implementing and solving the optimization problem, where neither globally optimal nor feasible solutions can be guaranteed.

## 3. Reactor optimization

### 3.1. Model

In this section, the application of the reduced microkinetic $C_1$ network for the optimization of a methane reforming reactor is presented. For this purpose, we make use of the previously proposed [1] and applied [2,33,34] methodology of Elementary Process Functions (EPF). This concept allows for a rigorous and apparatus independent optimization of chemical processes, only considering a representative matter element traveling through the process. As a result, a trajectory in the state space is identified which connects initial and final states of the fluid element, that are not necessarily fixed. In order to steer the matter element from its initial to the final point, the external fluxes acting at the matter element are used, in particular the mass and energy fluxes. In the beginning, we consider unlimited fluxes in order to identify the maximum performance potential of this process. According to our EPF concept, this first step is referred to as level 1. However, for the technical realization of the proposed process concept, unlimited fluxes are not feasible due to transport limitations. Thus, the influence of limited fluxes on the process performance is evaluated (level 2). In the end, this yields a technically feasible approximation of the process (level 3).

Here, the usage of the reduced microkinetic model with the EPF concept for level 1 is demonstrated. A sketch of the fluid element and the fluxes is shown in Fig. 7. The aim of the process is the production of a hydrogen rich product gas for low temperature fuel cell applications (e.g. PEM fuel cells). Hence, the objective is a maximum hydrogen concentration at the outlet of the reactor (Eq. (13)). However, the platinum catalyst in PEM fuel cells is known to be sensitive to carbon monoxide [35]. This yields an application related additional constraint for the optimization to ensure operability of the fuel cell (Eq. (23)). A maximum concentration of 10 ppm carbon monoxide shall not be exceeded. Another constraint is related to the rhodium catalyst (Eq. (22)). To obtain long term stability, temperatures above 1000 K need to be avoided. The just discussed two constraints are related to the chosen processes and materials, but do not originate from the EPF methodology directly.

To adequately describe this system, balance equations, thermodynamic models and kinetic rate expressions are needed. The optimization problem and the required equations are summarized in Table 4. To optimize the system, a dimensionless formulation of
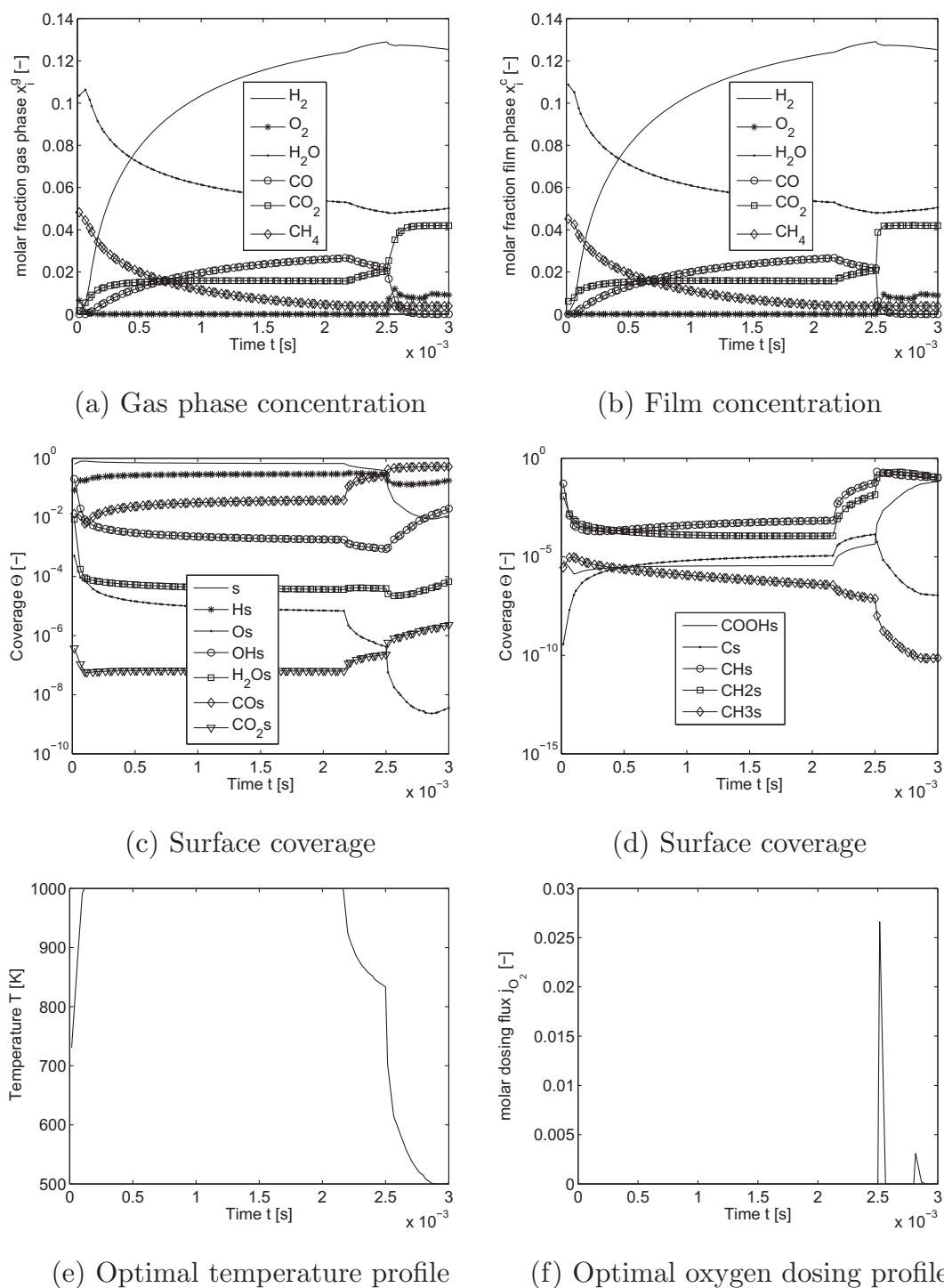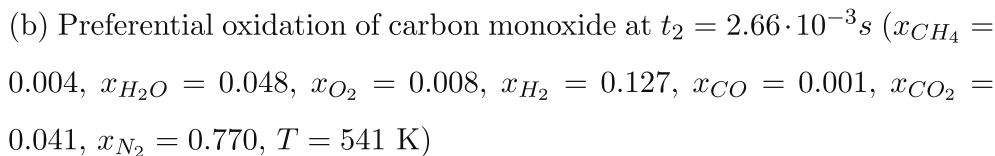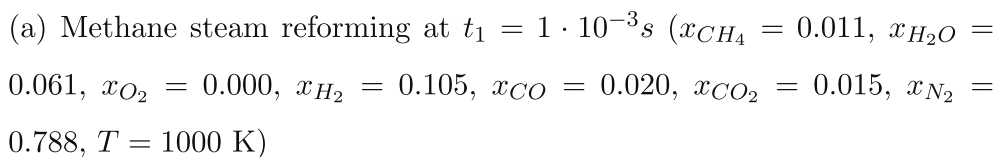


(a) Gas phase concentration

(b) Film concentration

(c) Surface coverage

(d) Surface coverage

(e) Optimal temperature profile

(f) Optimal oxygen dosing profile

**Fig. 8.** Optimization results.

(a) Methane steam reforming at $t_1 = 1 \cdot 10^{-3}s$ ($x_{CH_4} = 0.011$, $x_{H_2O} = 0.061$, $x_{O_2} = 0.000$, $x_{H_2} = 0.105$, $x_{CO} = 0.020$, $x_{CO_2} = 0.015$, $x_{N_2} = 0.788$, $T = 1000$ K)



(b) Preferential oxidation of carbon monoxide at $t_2 = 2.66 \cdot 10^{-3}s$ ($x_{CH_4} = 0.004$, $x_{H_2O} = 0.048$, $x_{O_2} = 0.008$, $x_{H_2} = 0.127$, $x_{CO} = 0.001$, $x_{CO_2} = 0.041$, $x_{N_2} = 0.770$, $T = 541$ K)

**Fig. 9.** Flux distributions at different times during the optimization.

**Table 3**
Comparison of different reduction methods.

**Table 4**
DAE constrained optimization problem: Maximum hydrogen concentration for PEM fuel cell applications.

| | | |
|---|---|---|
| Objective: | $\max\limits_{T(t),j_i(t)} x_{H_2}^{g,final}$ | (13) |
| Subject to: balances | $\dfrac{d(\epsilon x_i^g \hat{c}_t^g)}{d\tau} = -\hat{n}_i^{gc} + \hat{j}_i$ | (14) |
| | $\dfrac{d(\epsilon \hat{c}_t^g)}{d\tau} = -\hat{n}_t^{gc} + \hat{j}_t$ | (15) |
| | $0 = \hat{n}_i^{gc} + \dfrac{\sigma_i^c}{M_i c_{t,0}^g k_m^{ref}}$ | (16) |
| | $0 = \hat{n}_t^{gc} + \dfrac{1}{c_{t,0}^g k_m^{ref}} \sum\limits_{i=1}^{N_{Com}} \dfrac{\sigma_i^c}{M_i}$ | (17) |
| Kinetics | $\sigma_i^c = M_i \sum\limits_{j=1}^{N_{Com}} v_{i,j} r_j \quad r_j = r_j(T, x^c, \Theta)$ [14] | (18) |
| | $x_i^c - x_i^g = -\dfrac{1}{2\hat{c}_t^g} \sum\limits_{j=1}^{N_{Com}} \dfrac{\hat{n}_i^{gc}\left(x_j^c + x_j^g\right) - \hat{n}_j^{gc}\left(x_i^c + x_i^g\right)}{\hat{k}_{m,i,j}}$ | (19) |
| | $\hat{k}_{m,i,j} = \left(\dfrac{D_{i,j}}{D_{ref}}\right)^{1-n_{Sh}} \quad D = D(T,p)$ [36, p. 115] | (20) |
| Ideal gas law | $\hat{c}_t^g = \dfrac{p^g T_0}{p_0^g T}$ | (21) |
| Process constraints | $T \leqslant 1000\ K$ | (22) |
| | $x_{CO,final}^g \leqslant 1 \cdot 10^{-5}$ | (23) |

the component mass balance for all gas phase components ($CH_4$, $O_2$, $H_2$, $H_2O$, $CO$, $CO_2$, $N_2$) was used (Eq. (14)), which accounts for accumulation, mass transfer to the catalyst surface and external dosing of components. Further, a total mass balance is required (Eq. (15)). On the catalyst surface, the component mass balances (Eq. (16)) cover all adsorbed species (free surface sites (s), $H_s$, $O_s$, $OH_s$, $H_2O_s$, $CO_s$, $CO_{2,s}$, $COOH_s$, $C_s$, $CH_s$, $CH_{2,s}$, $CH_{3,s}$). The catalyst is assumed to operate at quasi-stationary conditions and the balance accounts for mass transfer between gas phase and catalyst, and a chemical source/sink, which includes the microkinetic model.

The mass transfer between gas phase and catalyst is described with the Maxwell–Stefan equations (Eq. (19)). The matrix of diffusion coefficients $D_{ij}$ was estimated with the help of literature correlations [36, p. 11.5]. The thermodynamic behavior of the system is described by ideal gas law (Eq. (21)).

As optimization variables the external mass fluxes $j_i$ of methane, water, and oxygen were chosen along with the optimal temperature profile.

To find the optimal solution, the DAE constrained optimization problem was discretized in time using orthogonal collocation on finite elements [37]. The resulting system of nonlinear algebraic equations was implemented in AMPL [38] and solved with the algorithm CONOPT [39]. Solving the optimization problem took roughly 22 min on a desktop computer (Intel(R) Core(TM)2 Duo E8400 CPU @ 3.00 GHz; Ubuntu 10.04 operating system, 2 GB memory).

**Table A.1**
Overall errors $(log_{10}(\epsilon^k))$ of removed reaction for catalytic partial oxidation of methane at different temperatures. Significant reactions are marked in gray.

| Reac. | 400K | 600K | 800K | 1000K | 1200K |
|---|---|---|---|---|---|
| 1 | -13.7 | -1.47 | -1.58 | -2.95 | -2.13 |
| 2 | -13.9 | -1.47 | -1.5 | -1.55 | -1.29 |
| 3 | -13.7 | -1.47 | -1.5 | -1.62 | -1.36 |
| 4 | -18.5 | -5.32 | -4.86 | -2.29 | -2.34 |
| 5 | -17.3 | -3.87 | -1.97 | -3.45 | -4.9 |
| 6 | -16.1 | -26.3 | -27.2 | -22.9 | -18.8 |
| 7 | -15.6 | -2.78 | -1.54 | -1.59 | -1.65 |
| 8 | -16.1 | -26.1 | -26 | -18.9 | -14.3 |
| 9 | -31 | -25.7 | -27.4 | -25.1 | -25.6 |
| 10 | 1.34 | -1.44 | -3.03 | -3.58 | -2.49 |
| 11 | -10.5 | -1.47 | -2.96 | -2.41 | -2.4 |
| 12 | -16.9 | -21.6 | -18.9 | -15 | -13.7 |
| 13 | -17.8 | -26.6 | -28.9 | -25.6 | -22.2 |
| 14 | -116 | -27.5 | -28.3 | -25.5 | -23.6 |
| 15 | -17 | -1.74 | -3.31 | -2.67 | -2.58 |
| 16 | -14.4 | -3.1 | -9.66 | -6.44 | -7.48 |
| 17 | -16.4 | -4.15 | -10.4 | -8.96 | -8.73 |
| 18 | -15.6 | -3.23 | -9.94 | -6.53 | -7.71 |
| 19 | -18 | -17.5 | -17.2 | -16.6 | -16.7 |
| 20 | -15.7 | -8.16 | -11.6 | -10.9 | -12.7 |
| 21 | -14.7 | -20 | -21.6 | -17.4 | -18.3 |
| 22 | -14.5 | -26.5 | -26.7 | -22.3 | -22.1 |
| 23 | -18.2 | -20 | -21.6 | -17.3 | -18.2 |
| 24 | -27.2 | -26.3 | -27.7 | -24.1 | -28.2 |
| 25 | -30.6 | -27 | -28.1 | -26.8 | -25.8 |
| 26 | -26.4 | -26.4 | -27.7 | -25.8 | -22.7 |
| 27 | -18.3 | -25.6 | -23 | -15.4 | -11.8 |
| 28 | -16.6 | -0.856 | -3.23 | -2.1 | -1.37 |
| 29 | -18.7 | -8.25 | -13.3 | -3.06 | -1.8 |
| 30 | -15.1 | -4.55 | -11 | -3.11 | -2.15 |
| 31 | -13.6 | -1.47 | -6.88 | -2.24 | -1.71 |
| 32 | -18.4 | -13.1 | -13.8 | -6.16 | -5.67 |
| 33 | -17.2 | -12.2 | -12.9 | -8.14 | -7.55 |
| 34 | -12 | -16.1 | -14.4 | -13.1 | -12.3 |
| 35 | -16.8 | -0.854 | -5.79 | -3.93 | -4.58 |
| 36 | -18.1 | -3.17 | -5.98 | -5.44 | -5.72 |
| 37 | -17.3 | -4.54 | -6.3 | -8.99 | -9.11 |
| 38 | -14.7 | -26 | -27.3 | -18.7 | -15.7 |
| 39 | -13.5 | -26.1 | -22.5 | -18 | -16.3 |
| 40 | -14.3 | -1.47 | -4.77 | -2.23 | -1.54 |
| 41 | -10.4 | -20.3 | -26.8 | -18.1 | -17.4 |

**Table A.2**
Overall errors $(log_{10}(\epsilon^k))$ of removed reaction for steam reforming of methane at different temperatures. Significant reactions are marked in gray.

| Reac. | 400K | 600K | 800K | 1000K | 1200K |
|---|---|---|---|---|---|
| 1 | -6.89 | -7.34 | -2.53 | -0.21 | -0.357 |
| 2 | -125 | -28.3 | -25.9 | -25.2 | -24 |
| 3 | -9.77 | -23.3 | -12.6 | -3.51 | -4.26 |
| 4 | -11 | -16.4 | -3.99 | -0.407 | -0.809 |
| 5 | -10.8 | -25.1 | -12.2 | -3.54 | -4.4 |
| 6 | -18 | -27.5 | -24.6 | -21.5 | -18.1 |
| 7 | -5.07 | -7.09 | -2.3 | -0.197 | -0.357 |
| 8 | -5.1 | -26.9 | -18.4 | -15.8 | -12.8 |
| 9 | -20.1 | -26.8 | -24.9 | -23 | -24 |
| 10 | -2.93 | 1.6 | 0.34 | -1.69 | -1.34 |
| 11 | 1.58 | -1.68 | -0.244 | -0.692 | -1.98 |
| 12 | -9.43 | -26.9 | -18.3 | -13.9 | -13.6 |
| 13 | -16.4 | -27.1 | -24.9 | -23.4 | -21.6 |
| 14 | -101 | -28.1 | -26.2 | -23.8 | -23 |
| 15 | -5.89 | -4.26 | 1.05 | -1.07 | -2.12 |
| 16 | -6.33 | -7.83 | -3.39 | -4.31 | -6.78 |
| 17 | -7.62 | -9.53 | -6.09 | -7.15 | -8.33 |
| 18 | -5.76 | -7.61 | -2.93 | -4.29 | -6.64 |
| 19 | -10.6 | -27 | -24.8 | -16.6 | -17.2 |
| 20 | -11 | -26.7 | -15.7 | -10.3 | -12.4 |
| 21 | -11 | -27.3 | -24.8 | -16.8 | -18 |
| 22 | -10.7 | -27 | -25.9 | -22.4 | -22.6 |
| 23 | -10.8 | -26.6 | -24.8 | -16.8 | -17.9 |
| 24 | -20.1 | -27.3 | -25 | -23.9 | -23 |
| 25 | -20 | -27.6 | -24.5 | -23 | -22.8 |
| 26 | -17.1 | -27.1 | -25.6 | -22.7 | -21.6 |
| 27 | -10.1 | -19.4 | -15.7 | -13.4 | -10.8 |
| 28 | -11 | -7.75 | -3.85 | -0.54 | -0.407 |
| 29 | -6.94 | -8.35 | -4.09 | -0.684 | -0.605 |
| 30 | -10.4 | -7.69 | -2.6 | -1.26 | -1.19 |
| 31 | -5.45 | -2.19 | -0.0657 | -0.3 | -0.46 |
| 32 | -10 | -21.8 | -15.4 | -5.71 | -5.45 |
| 33 | -10.4 | -24.7 | -16.9 | -8.2 | -7.47 |
| 34 | -11.1 | -23.2 | -13.2 | -12.2 |
| 35 | -10.8 | -8.08 | -4.56 | -3.13 | -4.18 |
| 36 | -10.9 | -7.58 | -2.42 | -5.22 | -5.51 |
| 37 | -5.49 | -13.7 | -5.18 | -8.96 | -9.03 |
| 38 | -10.6 | -27.3 | -22.1 | -19 | -15.1 |
| 39 | -7.43 | -27.5 | -24.9 | -18.2 | -16.2 |
| 40 | -5.41 | -4.38 | 0.862 | -0.29 | -0.385 |
| 41 | -2.33 | -10.8 | -9.8 | -17.7 | -16.9 |

**Table A.3**
Overall errors $(log_{10}(\epsilon^k))$ of removed reaction for dry reforming of methane at different temperatures. Significant reactions are marked in gray.

| Reac. | 400K | 600K | 800K | 1000K | 1200K |
|---|---|---|---|---|---|
| 1 | -4.46 | -6.44 | -1.13 | -1.44 | -2.65 |
| 2 | -134 | -27.3 | -21.1 | -20.8 | -1.37 |
| 3 | -6.72 | -20.7 | -5.13 | -4.36 | -1.32 |
| 4 | -5.73 | -16.9 | -1.55 | -0.942 | -2.08 |
| 5 | -6.71 | -22.8 | -4.82 | -4.14 | -4 |
| 6 | -18 | -27.3 | -21.4 | -20.7 | -18.4 |
| 7 | -5.12 | -8.47 | -0.573 | -0.708 | -1.33 |
| 8 | -5.73 | -26.8 | -19.7 | -16.1 | -14.5 |
| 9 | -19.4 | -28 | -21.7 | -20.9 | -23.5 |
| 10 | -1.55 | -8.65 | -0.573 | -0.165 | -2.14 |
| 11 | 1.6 | -8.59 | -0.573 | -0.165 | -3.43 |
| 12 | -7.25 | -27.5 | -14.8 | -17.1 | -13.7 |
| 13 | -17 | -27.1 | -22.4 | -22.1 | -21.4 |
| 14 | -84.6 | -27 | -22.1 | -20.9 | -22.8 |
| 15 | -8.14 | -9.26 | -0.931 | -0.549 | -3.66 |
| 16 | -5.03 | -9.1 | -1.54 | -3.71 | -7.17 |
| 17 | -5.8 | -10.3 | -2.51 | -4.85 | -8.98 |
| 18 | -5.13 | -8.55 | -0.983 | -3.47 | -7.09 |
| 19 | -7.31 | -27.5 | -17.1 | -16.9 | -16.5 |
| 20 | -5.73 | -19.5 | -7.08 | -9.22 | -11.5 |
| 21 | -5.71 | -27.2 | -15 | -15.8 | -17 |
| 22 | -6.75 | -27.7 | -21.5 | -20.7 | -20.5 |
| 23 | -8.14 | -27.3 | -15 | -15.7 | -16.9 |
| 24 | -19.1 | -27.8 | -21.9 | -20.7 | -23.7 |
| 25 | -18.2 | -26.9 | -21.7 | -23.2 | -23.6 |
| 26 | -18.8 | -27.5 | -21.4 | -20.9 | -22.7 |
| 27 | -7.52 | -22.4 | -17 | -13.2 | -12 |
| 28 | -5.77 | -9.45 | -2.35 | -0.435 | -1.5 |
| 29 | -6.09 | -9.45 | -2.45 | -0.526 | -2.04 |
| 30 | -6.72 | -8.3 | -2.52 | -1.06 | -2.24 |
| 31 | -1.56 | 1.55 | -0.715 | -0.258 | -1.9 |
| 32 | -7.58 | -20.1 | -8.82 | -5.66 | -5.21 |
| 33 | -5.7 | -22.9 | -12 | -8.02 | -7 |
| 34 | -7.42 | -27.1 | -17.3 | -13 | -11.7 |
| 35 | -8.32 | -17.2 | -4.19 | -3.35 | -4.33 |
| 36 | -5.72 | -10.3 | -3.84 | -5.15 | -5.36 |
| 37 | -5.79 | -15.8 | -6.6 | -8.22 | -8.75 |
| 38 | -7.14 | -27.3 | -18.2 | -16.7 | -15.6 |
| 39 | -5.66 | -26.8 | -21.5 | -18.1 | -15.7 |
| 40 | -5.09 | -10.1 | -1.25 | -0.219 | -1.72 |
| 41 | -3.6 | -12.2 | -8.47 | -14.5 | -16.8 |

**Table A.4**
Overall errors $(log_{10}(\epsilon^k))$ of removed reaction for water gas shift regime at different temperatures. Significant reactions are marked in gray.

| Reac. | 400K | 600K | 800K | 1000K | 1200K |
|---|---|---|---|---|---|
| 1 | -9.78 | -5.9 | -1.06 | 0.0179 | 0.0436 |
| 2 | -150 | -43 | -21.3 | -21.2 | -21.1 |
| 3 | -14.6 | -19.8 | -7.48 | -3.49 | -2.98 |
| 4 | -14.7 | -16.1 | -2.78 | -0.125 | -0.243 |
| 5 | -15.7 | -23.3 | -7.36 | -3.48 | -2.98 |
| 6 | -23.9 | -24.7 | -21.5 | -19.9 | -14.9 |
| 7 | -9.55 | -5.58 | -0.913 | 0.0254 | 0.0435 |
| 8 | -15.8 | -24.6 | -18.3 | -14 | -10.5 |
| 9 | -24 | -25.3 | -21.3 | -21 | -22.6 |
| 10 | -7.95 | -0.63 | -0.858 | 0.0281 | 0.0436 |
| 11 | -6.71 | -3.68 | -0.922 | 0.0261 | 0.0435 |
| 12 | -14.2 | -25.2 | -16.5 | -11.9 | -11.9 |
| 13 | -24.2 | -25.4 | -21.3 | -20.4 | -18 |
| 14 | -92.7 | -25.9 | -21.4 | -21.9 | -21.4 |
| 15 | -13.8 | -5.05 | -1.15 | -0.333 | -0.171 |
| 16 | -10.4 | -6.31 | -1.48 | -2.47 | -6.27 |
| 17 | -5.54 | -8.33 | -7.06 | -3.79 | -5.04 |
| 18 | -6.24 | -5.92 | -1.11 | -2.62 | -5.32 |
| 19 | -5.56 | -25.8 | -19.1 | -14.8 | -17.1 |
| 20 | -5.56 | -19.2 | -8.8 | -8.48 | -10.4 |
| 21 | -5.56 | -24.5 | -18.3 | -15.2 | -15.8 |
| 22 | -5.56 | -25.7 | -21.7 | -19.6 | -17.9 |
| 23 | -5.56 | -24.8 | -18.3 | -15.1 | -15.7 |
| 24 | -5.56 | -24.8 | -21.8 | -21.2 | -22 |
| 25 | -5.56 | -24.1 | -23.6 | -22 | -23.1 |
| 26 | -5.56 | -26.8 | -21.4 | -21.2 | -21.4 |
| 27 | -5.56 | -17.6 | -18.4 | -19 | -18.5 |
| 28 | -5.89 | -6.38 | -3.06 | -4.86 | -8.11 |
| 29 | -5.77 | -6.73 | -3.2 | -4.92 | -8.2 |
| 30 | -5.74 | -6.97 | -2.21 | -6.07 | -8.7 |
| 31 | 1.52 | 1.54 | 0.829 | -4.89 | -8.72 |
| 32 | -5.56 | -18.7 | -10.9 | -10.9 | -12.3 |
| 33 | -5.56 | -23 | -13.7 | -12.7 | -13.7 |
| 34 | -5.56 | -25.6 | -18.7 | -16.1 | -16 |
| 35 | -5.69 | -7.12 | -4.52 | -7.24 | -11.2 |
| 36 | -5.67 | -6.91 | -2.7 | -6.19 | -9.93 |
| 37 | -5.56 | -13.1 | -5.91 | -7.73 | -10.3 |
| 38 | -5.56 | -27.1 | -19.2 | -14.9 | -14.1 |
| 39 | -5.56 | -24.4 | -22 | -19.1 | -18.9 |
| 40 | -4.96 | -5.53 | -0.419 | -4.66 | -8.41 |
| 41 | -5.56 | -9.6 | -8.73 | -11.5 | -15.5 |

## 3.2. Results

According to the obtained optimal results (Fig. 8), the matter element initially starts at a moderate temperature (720 K) and is heated up until it reaches the maximum feasible temperature (1000 K). This accelerates the reaction and leads to a fast steam reforming of methane at high temperatures. Significant amounts of hydrogen and carbon monoxide are formed, while only a small quantity of carbon dioxide ($\leqslant 2\%$) is generated. No dosing of methane, water or oxygen is desirable during the steam reforming process, but all available methane and water should be fed at the reactor inlet. The catalyst surface mainly consists of free surface sites ($\geqslant 60\%$) due to the high process temperature. The most dominant species is dissociated hydrogen ($H_s$) with approx. 30%.

After methane steam reforming, a regime shift is initiated by rapidly reducing the temperature of the matter element from 1000 to 500 K and dosing of a discrete oxygen peak at a reduced temperature of approximately 830 K. The injection of oxygen at a higher temperature would result in combustion of hydrogen and partial or total oxidation of methane. At this reduced temperature, oxygen is mainly used for the reduction of the carbon monoxide concentration. This step is essential to ensure an output concentration of 10 ppm or less for the further use of the product gas in low temperature PEM fuel cells. Also, small amounts of hydrogen and methane are oxidatively converted as can be seen from the gas phase concentration profiles. The concentration of carbon monoxide is reduced by preferential oxidation from 2.7% to 10 ppm. The amount of carbon dioxide increases from 1.6 to 4.2%. During the preferential oxidation the temperature is decreasing monotonically. This does not only prevent the parallel oxidation of the

**Table A.5**
Overall errors $(log_{10}(\epsilon^k))$ of removed reaction for hydrogen combustion at different temperatures. Significant reactions are marked in gray. The rates of reactions 10 to 41 is zero because no carbon is available in this regime.

| Reac. | 400K | 600K | 800K | 1000K | 1200K |
|---|---|---|---|---|---|
| 1 | -1.22 | -1.42 | -1.41 | -1.34 | -1.33 |
| 2 | -1.22 | -1.42 | -1.41 | -1.34 | -1.33 |
| 3 | -1.62 | -1.45 | -1.41 | -1.37 | -1.4 |
| 4 | -1.27 | -2.18 | -1.99 | -1.65 | -1.59 |
| 5 | -3.76 | -1.61 | -2.47 | -3.12 | -3.38 |
| 6 | -21.5 | -27.6 | -24.5 | -22.5 | -18 |
| 7 | -1.22 | -1.42 | -1.41 | -1.34 | -1.33 |
| 8 | -21.1 | -26.8 | -23.8 | -18.5 | -14.6 |
| 9 | -20.7 | -27.3 | -51.9 | -25.7 | -24.1 |
| 10 | $-\infty$ | $-\infty$ | $-\infty$ | $-\infty$ | $-\infty$ |
| 11 | $-\infty$ | $-\infty$ | $-\infty$ | $-\infty$ | $-\infty$ |
| 12 | $-\infty$ | $-\infty$ | $-\infty$ | $-\infty$ | $-\infty$ |
| 13 | $-\infty$ | $-\infty$ | $-\infty$ | $-\infty$ | $-\infty$ |
| 14 | $-\infty$ | $-\infty$ | $-\infty$ | $-\infty$ | $-\infty$ |
| 15 | $-\infty$ | $-\infty$ | $-\infty$ | $-\infty$ | $-\infty$ |
| 16 | $-\infty$ | $-\infty$ | $-\infty$ | $-\infty$ | $-\infty$ |
| 17 | $-\infty$ | $-\infty$ | $-\infty$ | $-\infty$ | $-\infty$ |
| 18 | $-\infty$ | $-\infty$ | $-\infty$ | $-\infty$ | $-\infty$ |
| 19 | $-\infty$ | $-\infty$ | $-\infty$ | $-\infty$ | $-\infty$ |
| 20 | $-\infty$ | $-\infty$ | $-\infty$ | $-\infty$ | $-\infty$ |
| 21 | $-\infty$ | $-\infty$ | $-\infty$ | $-\infty$ | $-\infty$ |
| 22 | $-\infty$ | $-\infty$ | $-\infty$ | $-\infty$ | $-\infty$ |
| 23 | $-\infty$ | $-\infty$ | $-\infty$ | $-\infty$ | $-\infty$ |
| 24 | $-\infty$ | $-\infty$ | $-\infty$ | $-\infty$ | $-\infty$ |
| 25 | $-\infty$ | $-\infty$ | $-\infty$ | $-\infty$ | $-\infty$ |
| 26 | $-\infty$ | $-\infty$ | $-\infty$ | $-\infty$ | $-\infty$ |
| 27 | $-\infty$ | $-\infty$ | $-\infty$ | $-\infty$ | $-\infty$ |
| 28 | $-\infty$ | $-\infty$ | $-\infty$ | $-\infty$ | $-\infty$ |
| 29 | $-\infty$ | $-\infty$ | $-\infty$ | $-\infty$ | $-\infty$ |
| 30 | $-\infty$ | $-\infty$ | $-\infty$ | $-\infty$ | $-\infty$ |
| 31 | $-\infty$ | $-\infty$ | $-\infty$ | $-\infty$ | $-\infty$ |
| 32 | $-\infty$ | $-\infty$ | $-\infty$ | $-\infty$ | $-\infty$ |
| 33 | $-\infty$ | $-\infty$ | $-\infty$ | $-\infty$ | $-\infty$ |
| 34 | $-\infty$ | $-\infty$ | $-\infty$ | $-\infty$ | $-\infty$ |
| 35 | $-\infty$ | $-\infty$ | $-\infty$ | $-\infty$ | $-\infty$ |
| 36 | $-\infty$ | $-\infty$ | $-\infty$ | $-\infty$ | $-\infty$ |
| 37 | $-\infty$ | $-\infty$ | $-\infty$ | $-\infty$ | $-\infty$ |
| 38 | $-\infty$ | $-\infty$ | $-\infty$ | $-\infty$ | $-\infty$ |
| 39 | $-\infty$ | $-\infty$ | $-\infty$ | $-\infty$ | $-\infty$ |
| 40 | $-\infty$ | $-\infty$ | $-\infty$ | $-\infty$ | $-\infty$ |
| 41 | $-\infty$ | $-\infty$ | $-\infty$ | $-\infty$ | $-\infty$ |

**Table A.6**
Overall errors ($log_{10}(\epsilon^k)$) of removed reaction for carbon monoxide oxidation at different temperatures. Significant reactions are marked in gray.

| Reac. | 400K | 600K | 800K | 1000K | 1200K |
|---|---|---|---|---|---|
| 1 | -16.9 | -23.1 | -22.9 | -29.6 | -25.2 |
| 2 | -7.34 | -2.6 | -0.535 | -0.535 | -0.535 |
| 3 | -16.7 | -22.8 | -23.7 | -27.2 | -25.2 |
| 4 | -16 | -22.5 | -24.4 | -29.3 | -25.1 |
| 5 | -16 | -22.5 | -24 | -27.2 | -25.1 |
| 6 | -17 | -25.5 | -25.9 | -28.7 | -25 |
| 7 | -16.5 | -21.8 | -23.1 | -28.3 | -25.2 |
| 8 | -16.4 | -22.8 | -23.7 | -27.2 | -25.1 |
| 9 | -16.2 | -25.6 | -23.3 | -21.8 | -16.5 |
| 10 | -7.34 | -2.6 | -0.535 | -0.535 | -0.535 |
| 11 | -0.5 | -2.6 | -0.535 | -0.535 | -0.535 |
| 12 | -8.07 | -2.72 | -0.535 | -0.535 | -0.535 |
| 13 | -15.9 | -25.2 | -22.8 | -28.5 | -25.1 |
| 14 | -112 | -39.5 | -29.7 | -29.3 | -25.2 |
| 15 | -16.7 | -23 | -24.9 | -27.2 | -25.1 |
| 16 | -15.9 | -21.6 | -18.5 | -28.3 | -25.2 |
| 17 | -17.7 | -23.4 | -24 | -27.3 | -25 |
| 18 | -18 | -24.9 | -22.8 | -27.1 | -25.2 |
| 19 | -16.5 | -22.8 | -23.3 | -27.3 | -25 |
| 20 | -16.5 | -23.5 | -29.3 | -27.3 | -25.2 |
| 21 | -16.6 | -22.7 | -26.9 | -28.7 | -25.1 |
| 22 | -16.8 | -22.7 | -25.7 | -28.7 | -25.2 |
| 23 | -16.3 | -25.9 | -31.5 | -27.2 | -25.1 |
| 24 | -17 | -25.4 | -29 | -27.3 | -25.2 |
| 25 | -16.2 | -26.2 | -30.1 | -50.6 | -25.1 |
| 26 | -69.3 | -40.4 | -112 | -141 | -125 |
| 27 | -82.7 | -70.8 | -148 | -193 | -125 |
| 28 | -77.4 | -74.1 | -158 | -196 | -129 |
| 29 | -69.3 | -70.9 | -130 | -143 | -127 |
| 30 | -16 | -22.6 | -86.1 | -143 | -25.2 |
| 31 | -16.2 | -13.8 | -22.9 | -28.6 | -25.2 |
| 32 | -69.3 | -70.1 | -130 | -143 | -126 |
| 33 | -16.3 | -23.1 | -55.7 | -141 | -25.2 |
| 34 | -17 | -23.5 | -25.4 | -28.9 | -25.1 |
| 35 | -80 | -95.9 | -153 | -195 | -174 |
| 36 | -80 | -26.2 | -111 | -141 | -124 |
| 37 | -16.4 | -22.9 | -29.7 | -28.7 | -25.1 |
| 38 | -7.84 | -3.94 | -10.3 | -14.6 | -13.6 |
| 39 | -16.8 | -22.5 | -24 | -27.3 | -25.1 |
| 40 | -16 | -22.4 | -23.9 | -28.8 | -25 |
| 41 | 1.55 | 1.55 | -10.6 | -14.7 | -15.5 |

**Table A.7**
Overall errors ($log_{10}(\epsilon^k)$) of removed reaction for an equimolar gas mixture at different temperatures. Significant reactions are marked in gray.

| Reac. | 400K | 600K | 800K | 1000K | 1200K |
|---|---|---|---|---|---|
| 1 | -4.49 | -2.26 | -1.94 | -2.36 | -4.69 |
| 2 | -7.58 | -1.54 | -1.57 | -1.52 | -1.43 |
| 3 | -7.38 | -1.65 | -1.48 | -1.44 | -1.37 |
| 4 | -6.55 | -4.8 | -2.66 | -2.29 | -2.18 |
| 5 | -8.25 | -3.84 | -3.38 | -3.82 | -4.13 |
| 6 | -18.7 | -25.1 | -24.7 | -22.7 | -18 |
| 7 | -1.81 | -2.26 | -1.93 | -1.83 | -1.58 |
| 8 | -7.6 | -25.2 | -24.3 | -18.3 | -14.1 |
| 9 | -15.9 | -71.2 | -51.5 | -24.9 | -24.9 |
| 10 | -0.0733 | -1.68 | -1.92 | -2.22 | -5.53 |
| 11 | 1.46 | -1.54 | -1.9 | -2.02 | -2.34 |
| 12 | -9.2 | -19.7 | -16.7 | -14.5 | -13.4 |
| 13 | -15.9 | -25.4 | -24.4 | -23.9 | -21.5 |
| 14 | -85 | -24.6 | -24.8 | -24.4 | -26 |
| 15 | -7.6 | -1.93 | -2.17 | -2.31 | -2.57 |
| 16 | -2.62 | -2.72 | -3.87 | -5.58 | -7.46 |
| 17 | -4.25 | -5.31 | -6.46 | -8.38 | -9.48 |
| 18 | -1.83 | -2.83 | -3.87 | -5.58 | -7.56 |
| 19 | -5.81 | -16.2 | -16.5 | -16.3 | -16 |
| 20 | -8.04 | -7.06 | -8.32 | -10.2 | -11.9 |
| 21 | -7.47 | -17.2 | -15.8 | -16.7 | -17.5 |
| 22 | -7.61 | -24.9 | -23.1 | -21.7 | -20.7 |
| 23 | -7.6 | -17.2 | -15.8 | -16.7 | -17.4 |
| 24 | -16.5 | -24.4 | -24.8 | -24.2 | -25.5 |
| 25 | -16.3 | -27 | -25.7 | -24.5 | -24.5 |
| 26 | -17.4 | -24.3 | -24.9 | -24.2 | -24.9 |
| 27 | -7.83 | -25.8 | -22.2 | -16.2 | -12.4 |
| 28 | -7.66 | -3.32 | -5.23 | -3.1 | -1.89 |
| 29 | -8.22 | -11 | -6.48 | -3.46 | -2.28 |
| 30 | -7.52 | -5.21 | -6.57 | -4.05 | -2.75 |
| 31 | 0.392 | -1.54 | -3.8 | -3.41 | -2.52 |
| 32 | -7.34 | -14.7 | -10.4 | -7.12 | -5.65 |
| 33 | -8.26 | -12.8 | -12.8 | -9.47 | -7.52 |
| 34 | -5.66 | -16.9 | -17.9 | -14.4 | -12.3 |
| 35 | -7.74 | -3.32 | -5.52 | -4.7 | -4.67 |
| 36 | -7.23 | -3.64 | -7.51 | -6.59 | -5.81 |
| 37 | -6.49 | -6.06 | -11.2 | -10.1 | -9.19 |
| 38 | -7.96 | -24.8 | -24 | -21.1 | -16.2 |
| 39 | -7.69 | -25.2 | -24.1 | -19.4 | -16.2 |
| 40 | -2.67 | -2.79 | -3.24 | -2.77 | -2.01 |
| 41 | -1.86 | -17 | -16.8 | -18.4 | -17.9 |

desired hydrogen but also affects the equilibrium of the water gas shift reaction to further convert carbon monoxide and water to carbon dioxide and hydrogen. The regime shift is most apparent on the catalyst surface, where the composition changes drastically. Due to the lower temperature, the portion of free active sites gradually decreases, while the dehydrogenated methane species (especially $CH_{2,s}$ and $CH_s$) are more dominant. Also, an increased amount of adsorbed carboxylic groups (COOH) on the surface is obtained.

Due to the chemical regime shift from methane steam reforming to water gas shift reaction and preferential oxidation of carbon monoxide, also the flux distribution in the reaction network changes significantly as illustrated in Fig. 9. Here, the individual net (sum of forward and backward) reaction rates and their directions are shown for a typical steam reforming (Fig. 9(a)) and preferential oxidation (Fig. 9(b)) regime.

During steam reforming, major parts of the reaction network are active. The conversion of methane proceeds via dissociative adsorption on the catalyst surface and a further dehydrogenation to carbon, which then forms carbon monoxide and carbon dioxide. The required oxygen is provided by water dissociation, whereby large amounts of hydrogen are formed. As oxygen is not fed to the system and therefore is not present in the gas phase, oxygen adsorption/desorption on the catalyst surface basically does not take place.

During the preferential oxidation of carbon monoxide, the flux distribution in the reaction network changes significantly. First of all, oxygen adsorption is the fastest step in the reaction network and methane is no longer consumed. The reaction pathway for methane has even turned towards methanation, but the reaction rates are rather small and no significant methane generation takes place according to the methane concentration profile (Fig. 8). To convert carbon monoxide to carbon dioxide, CO reacts with $OH_s$ either directly or via an adsorbed carboxylic group to carbon dioxide, but the direct oxidation of CO with $O_s$ does not take place. Due to the changed reaction conditions, hydrogen also re-adsorbs on the Rhodium surface and is being oxidized to water.

The optimal results have been validated with the original reaction network. Under identical temperature and dosing profiles, the final molar fraction for hydrogen was 12.54%, which differs by $\Delta x_{H_2}^g = 0.016\%$ (relative error: 0.13%) from the value determined with the reduced reaction network ($x_{H_2}^{g,final,*} = 12.53\%$).

## 4. Conclusion

In this contribution, a new method for the reduction of complex microkinetic networks that consider elementary steps is proposed and illustrated. This is especially helpful for the optimization of chemical reactors, where on the one hand detailed rate expressions are desirable that are valid and accurate over large ranges of temperature, pressure, and composition. On the other hand simple and manageable models with favorable numerical properties especially regarding scaling and model complexity are desired.

For our proposed reduction method, emphasis is put on the resulting error between the original and the reduced reaction model to ensure quantitative agreement. A sensitivity study was performed to determine the influence of every reaction step on the flux distribution in the network at different chemical regimes. This reduction technique was applied to a microkinetic reaction network for $C_1$ chemistry [14]. The original and reduced networks

were further compared and a validation showed an average overall error of less than 0.05% in the predicted production rates.

Because of its general formulation, this reduction technique is also applicable to other chemical or biochemical reaction networks of arbitrary complexity and structure. This reduction method is easy to implement and no additional solver or optimization packages are required. Compared to other methods, we directly focus on the overall network error that is introduced by the modified network, rather than only taking the magnitude of the reactions in account, while fulfillment of the mass balance is still ensured. A single parameter $\epsilon^{crit}$ steers the degree of reduction in the number of reactions and the number of components.

The reduced reaction network was successfully used to derive an optimal methane reforming reactor for fuel cell applications based on dynamic optimization. The results indicate a segmented reactor concept with isothermal methane steam reforming at high temperature in the beginning and an oxygen dosing strategy and temperature reduction for the preferential oxidation of carbon monoxide to carbon dioxide afterwards. It was further shown that the reaction flux distribution in the network significantly changes due to the different chemical regimes, which further emphasizes the need of adequate microkinetic reaction models for the reliable optimal design of chemical reactors.

## Acknowledgments

## Appendix A. Significance of individual reactions in different chemical regimes

See Tables A1–A7.

## References

[1] H. Freund, K. Sundmacher, Towards a methodology for the systematic analysis and design of efficient chemical processes part 1. From unit operations to elementary process functions, Chem. Eng. Process. 47 (2008) 2051–2060.

[2] A. Peschel, H. Freund, K. Sundmacher, Methodology for the design of optimal chemical reactors based on the concept of elementary process functions, Ind. Eng. Chem. Res. 49 (2010) 10535–10548.

[3] K. Rasim, M. Bobeth, W. Pompe, N. Seriani, A microkinetic model of ammonia decomposition on a Pt overlayer on Au(1 1 1), J. Mol. Catal. A Chem. 325 (2010) 15–24.

[4] J. Sjoblom, D. Creaser, New approach for microkinetic mean-field modelling using latent variables, Comput. Chem. Eng. 31 (2007) 307–317.

[5] B. Sawatmongkhon, A. Tsolakis, K. Theinnoi, A.P.E. York, P.J. Millington, R.R. Rajaram, Microkinetic modelling for selective catalytic reduction (SCR) of NO$_x$ by propane in a silver-based automotive catalytic converter, Appl. Catal. B Environ. 111 (2012) 165–177.

[6] T.C. Brueggemann, D.G. Vlachos, F.J. Keil, Microkinetic modeling of the fast selective catalytic reduction of nitrogen oxide with ammonia on H-ZSM5 based on first principles, J. Catal. 283 (2011) 178–191.

[7] O. Korup, C.F. Goldsmith, G. Weinberg, M. Geske, T. Kandemir, R. Schloegl, R. Horn, Catalytic partial oxidation of methane on platinum investigated by spatial reactor profiles, spatially resolved spectroscopy, and microkinetic modeling, J. Catal. 297 (2013) 1–16.

[8] D.W. Blaylock, Y.-A. Zhu, W.H. Green, Computational investigation of the thermochemistry and kinetics of steam methane reforming over a multi-faceted nickel catalyst, Top. Catal. 54 (2011) 828–844.

[9] D. Chen, R. Lodeng, H. Svendsen, A. Holmen, Hierarchical multiscale modeling of methane steam reforming reactions, Ind. Eng. Chem. Res. 50 (2011) 2600–2612.

[10] A.K. Avetisov, J.R. Rostrup-Nielsen, V.L. Kuchaev, J.H.B. Hansen, A.G. Zyskin, E.N. Shapatina, Steady-state kinetics and mechanism of methane reforming with steam and carbon dioxide over Ni catalyst, J. Mol. Catal. A Chem. 315 (2010) 155–162.

[11] D.W. Blaylock, T. Ogura, W.H. Green, G.J.O. Beran, Computational investigation of thermochemistry and kinetics of steam methane reforming on Ni(1 1 1) under realistic conditions, J. Phys. Chem. C 113 (2009) 4898–4908.

[12] J. Sun, J.W. Thybaut, G.B. Marin, Microkinetics of methane oxidative coupling, Catal. Today 137 (2008) 90–102.

[13] N. Rankovic, A. Nicolle, D. Berthout, P. Da Costa, Kinetic modeling study of the oxidation of carbon monoxide-hydrogen mixtures over Pt/Al$_2$O$_3$ and Rh/Al$_2$O$_3$ catalysts, J. Phys. Chem. C 115 (2011) 20225–20236.

[14] M. Maestri, D.G. Vlachos, A. Beretta, G. Groppi, E. Tronconi, A C$_1$ microkinetic model for methane conversion to syngas on Rh/Al$_2$O$_3$, AICHE J. 55 (2009) 993–1008.

[15] A.B. Mhadeshwar, D.G. Vlachos, A catalytic reaction mechanism for methane partial oxidation at short contact times, reforming, and combustion, and for oxygenate decomposition and oxidation on platinum, Ind. Eng. Chem. Res. 46 (2007) 5310–5324.

[16] A. Mhadeshwar, D. Vlachos, Hierarchical multiscale mechanism development for methane partial oxidation and reforming and for thermal decomposition of oxygenates on Rh, J. Phys. Chem. B 109 (2005) 16819–16835.

[17] P. Aghalayam, Y. Park, N. Fernandes, V. Papavassiliou, A. Mhadeshwar, D. Vlachos, A C$_1$ mechanism for methane oxidation on platinum, J. Catal. 213 (2003) 23–38.

[18] D. Livio, A. Donazzi, A. Beretta, G. Groppi, P. Forzatti, Optimal design of a CPO-reformer of light hydrocarbons with honeycomb catalyst: effect of frontal heat dispersions on the temperature profiles, Top. Catal. 54 (2011) 866–872.

[19] A. Beretta, A. Donazzi, D. Livio, M. Maestri, G. Groppi, E. Tronconi, P. Forzatti, Optimal design of a CH$_4$ CPO-reformer with honeycomb catalyst: combined effect of catalyst load and channel size on the surface temperature profile, Catal. Today 171 (2011) 79–83.

[20] Z. Ulissi, V. Prasad, D.G. Vlachos, Effect of multiscale model uncertainty on identification of optimal catalyst properties, J. Catal. 281 (2011) 339–344.

[21] J.W. Thybaut, J. Sun, L. Olivier, A.C. Van Veen, C. Mirodatos, G.B. Marin, Catalyst design based on microkinetic models: Oxidative coupling of methane, Catal. Today 159 (2011) 29–36.

[22] R. Quiceno, O. Deutschmann, J. Warnatz, J. Perez-Ramirez, Rational modeling of the CPO of methane over platinum gauze – elementary gas-phase and surface mechanisms coupled with flow simulations, Catal. Today 119 (2007) 311–316.

[23] C. Jacobsen, S. Dahl, A. Boisen, B. Clausen, H. Topsoe, A. Logadottir, J. Norskov, Optimal catalyst curves: connecting density functional theory calculations with industrial reactor design and catalyst selection, J. Catal. 205 (2002) 382–387.

[24] F. Perini, J.L. Brakora, R.D. Reitz, G. Cantore, Development of reduced and optimized reaction mechanisms based on genetic algorithms and element flux analysis, Combust. Flame 159 (2012) 103–119.

[25] K. He, I.P. Androulakis, M.G. Ierapetritou, On-the-fly reduction of kinetic mechanisms using element flux analysis, Chem. Eng. Sci. 65 (2010) 1173–1184.

[26] A. Mitsos, G.M. Oxberry, P.I. Barton, W.H. Green, Optimal automatic reaction and species elimination in kinetic mechanisms, Combust. Flame 155 (2008) 118–132.

[27] A. Mhadeshwar, D. Vlachos, Is the water-gas shift reaction on Pt simple? Computer-aided microkinetic model reduction, lumped rate expression, and rate-determining step, Catal. Today 105 (2005) 162–172.

[28] I. Fishtik, C. Callaghan, R. Datta, Reaction route graphs. I. Theory and algorithm, J. Phys. Chem. B 108 (2004) 5671–5682.

[29] I. Fishtik, C. Callaghan, R. Datta, Reaction route graphs. II. Examples of enzyme- and surface-catalyzed single overall reactions, J. Phys. Chem. B 108 (2004) 5683–5697.

[30] I. Fishtik, C. Callaghan, R. Datta, Reaction route graphs. III. Non-minimal kinetic mechanisms, J. Phys. Chem. B 109 (2005) 2710–2722.

[31] P. Stoltze, Microkinetic simulation of catalytic reactions, Progr. Surf. Sci. 65 (2000) 65–150.

[32] Douglas C. Montgomery, George C. Runger, Norma F. Hubele, Engineering Statistics, third ed., Wiley, 2003. ISBN: 0471448540, 9780471448549, 480 p.

[33] H. Freund, A. Peschel, K. Sundmacher, Model-based reactor design based on the optimal reaction route, Chem. Ing. Tech. 83 (2011) 420–426.

[34] A. Peschel, F. Karst, H. Freund, K. Sundmacher, Analysis and optimal design of an ethylene oxide reactor, Chem. Eng. Sci. 66 (2011) 6453–6469.

[35] S. Kirsch, R. Hanke-Rauschenbach, B. Stein, R. Kraume, K. Sundmacher, The electro-oxidation of H$_2$CO in a model PEM fuel cell: oscillations, chaos, pulses, J. Electrochem. Soc. 160 (2013) F436–F446.

[36] B. Poling, J. Prausnitz, J. Connell, The Properties of Gases and Liquids, McGraw Hill, New York, 2007.

[37] A. Cervantes, L. Biegler, Large-scale DAE optimization using a simultaneous NLP formulation, AIChE J. 44 (1998) 1038–1050.

[38] R. Fourer, D. Gay, B. Kernighan, AMPL: A Modeling Language for Mathematical Programming, Thomson/Brooks/Cole, 2003.

[39] A. Drud, CONOPT: a large-scale GRG code, ORSA J. Comput. 6 (1994) 207–216.